

# A study on the tensile response and fracture in carbon nanotube-based composites using molecular mechanics

Vineet V. Mokashi, Dong Qian<sup>\*</sup>, Yijun Liu

*Department of Mechanical, Industrial and Nuclear Engineering, P.O. Box 210072, University of Cincinnati, Cincinnati, OH 45221-0072, USA*

Received 11 May 2006; received in revised form 10 August 2006; accepted 16 August 2006

Available online 9 October 2006

## Abstract

A study on the mechanical properties of polyethylene and carbon nanotube (CNT) based composites is presented using molecular mechanics simulations. The systems being investigated consist of amorphous as well as crystalline polyethylene (PE) composites with embedded single-walled CNTs. All the systems are subjected to quasi-static tensile loading, with the assumption that no cross-link chemical bonds exist between the CNT and polyethylene matrix in the case of nanocomposites. Based on the numerical simulations, we report Young's moduli ( $C_{33}$ ) of 212–215 GPa for crystalline PE, which closely match the experimental measurement. Furthermore, elastic stiffness of 3.19–3.69 GPa and tensile strength of 0.21–0.25 GPa are obtained for amorphous PE. The tensile responses are found to be highly isotropic. In the case of crystalline PE reinforced by long through CNTs, moderate improvements in the tensile strength and elastic stiffness are observed. However, the results differ from the predictions using the rule of mixtures. On the other hand, although significant increase in the overall tensile properties is observed when amorphous PE is reinforced by long through CNTs, the load transfer at the nanotube/polymer interface has negligible effect. Finally, degradations in both tensile strength and elastic stiffness are reported when amorphous PE is reinforced by embedded CNTs. The study presented indicates the importance of specific CNT and polymer configurations on the overall properties of the nanocomposite.

© 2006 Elsevier Ltd. All rights reserved.

*Keywords:* Carbon nanotubes; Polymer composite; Nanocomposites; Polyethylene; Tensile strength

## 1. Introduction

Carbon nanotubes (CNTs) have been the focus of research since their discovery in 1991 by Iijima [1]. They are currently being investigated for applications in many conventional and unprecedented areas, including light-weight structural composites, field emission devices, electronics, nano-electro-mechanical devices, sensors, actuators, gas storage, medical applications and nano-robotics (see, e.g., reviews in [2,3], also [4] for potential applications of CNTs). Due to its exceptionally high stiffness, strength, resilience, as well as superior electrical and thermal properties, CNTs may become ideal reinforcing materials for an entirely new class of composites. It has been demonstrated

that with just 1% (by weight) of CNTs added in a matrix, the stiffness of the resulting composite film can increase between 36% and 42% and the tensile strength by 25% [5]. The load carrying capacities of CNTs in composites have also been demonstrated in some experiments [5–8] and preliminary simulations [9–11].

While significant efforts [5,8,12–15] have been made, directly characterizing the mechanics in CNT-based nanocomposites at nanometer scale is still a challenging task. On the other hand, simulations based on both discrete and continuum models have provided useful insight into the mechanics of CNT-based nanocomposites. *Discrete* models, such as molecular dynamics (MD) simulations have been widely used. Frankland et al. [16,17] have studied the effects of both non-bonded interaction and cross-linking on the load transfer capabilities at the CNT–polymer interface. A virtual pull-out test on

<sup>\*</sup> Corresponding author. Tel.: +1 513 556 0422; fax: +1 513 556 3390.  
E-mail address: [Dong.Qian@uc.edu](mailto:Dong.Qian@uc.edu) (D. Qian).

CNT-based polymers is reported in Frankland et al. [18]. The material system studied is similar to what is being investigated in this paper, although our work focuses more on the failure aspect and overall mechanical properties. Griebel and Hamaekers [19] have used molecular dynamic to evaluate the elastic properties of single-walled CNT-based nanocomposites. Their simulation results show some agreement with the results by using the rule of mixtures. The *continuum model* has also been applied for analyzing the mechanical responses of nanocomposites. Pipes and Hubert have proposed a mechanics model based on the notion of self-similarity [20]. Odegard developed a continuum model by introducing the representative volume element [21]. The continuum model is established by equating the strain energy of the continuum to the potential energy of the discrete polymer system. Specific case of load conditions such as bending is then examined to obtain the continuum properties. Liu and Chen developed finite element and boundary element approaches [9,10]. In their method, the CNT is modeled as a thin elastic layer in the form of either a capsule or open cylinder. Finite element approach has also been employed by Fisher et al. [22,23] to study the effect of waviness of the CNT on the mechanical properties. A multiscale approach has been implemented by Li and Chou [24] for studying the load transfer in CNT-reinforced composites. In this approach, CNTs are modeled using molecular mechanics and polymer matrix is modeled using finite element method. The CNT/polymer interface is assumed to be either perfectly bonded or governed by the van der Waals interaction. The rule of mixture is observed to hold for axial elastic modulus.

The main objective of this paper is to investigate the tensile response and fracture behavior of polyethylene (PE) reinforced by single-walled CNTs. The methods of MD and MM have been extensively applied in the study of fracture in material systems such as metals, semiconductors and CNTs. In several successful applications of MD described earlier, the attention has been focused on the overall elastic properties and interfacial mechanics. In the present work, fractures in CNT-reinforced composites are simulated with the use of MM. MM is different from MD in that it seeks to resolve the equilibrium condition of the system by minimizing the potential energy, while in MD the equation of motion is solved based on certain time integration scheme.

The equilibrium of the nanocomposite system is closely tied to the interatomic interactions. In MM simulation, these interactions can be divided into two categories. The first is the bonded interaction. We have used Brenner potential [25] to model the carbon–carbon bond in CNTs, and the DL\_POLY force field model [26] for the hydrocarbon bond within the polymers. The non-bonded interactions between the molecules are governed by the widely used Lennard–Jones potential. It should be noted that the chemical structure of polyethylene polymer is categorized as a linear polymer in which the  $-\text{CH}_2-\text{CH}_2-$  unit is

repeated along a chain. This is one of the simplest forms of the polymers. Other forms of polymers, such as branched structures (linear chain with side additions) and cross-linked structures (linkage between the chains), are also known to be common. A robust force field model, such as the one being used here, should be able to capture the essence of the interatomic interactions involved in all of these structures.

The properties of various polymer systems, subject to tensile boundary conditions, and the change in properties due to CNT reinforcement are the main focuses of this study. To be more specific, we have studied the fracture behavior of five systems: the crystalline and amorphous composite systems, the crystalline and amorphous composite systems that are reinforced by long through CNTs, and amorphous composite systems that are reinforced by short CNTs. For all of the systems considered, no further functionalization process is considered and therefore no cross-link chemical bond exists between the CNT and the polymer. The mechanical behaviors of the above systems, particularly the fracture, are obtained through the MM simulations.

The remainder of the paper is organized as follows. In Section 2, interatomic and intermolecular potentials used to model the polymer and composite systems are presented. In Section 3, the structures and models used for this study are described. The concepts of MM, quasi-static simulations and equilibrium solution are explained in Section 4. The details on the simulation setup and results are given in Section 5. Finally, in Section 6, conclusions are made and the scope for future investigations is also discussed.

## 2. Force fields and molecular potentials

The expression for the total energy of the CNT–PE composite system is written as:

$$E_{\text{total}} = E_{\text{CNT}} + E_{\text{polymer}} + E_{\text{intermolecular}}, \quad (1)$$

where  $E_{\text{total}}$  is the total energy of the system,  $E_{\text{CNT}}$  is the potential energy of the CNT,  $E_{\text{polymer}}$  is the energy of the polymer matrix and  $E_{\text{intermolecular}}$  is the energy of interaction between the CNT and the polymer matrix. The models for these components are described next.

### 2.1. Potential model for carbon nanotubes

The empirical bond order potential proposed by Brenner [25] is used for modeling the CNTs. The equation for the Brenner potential is given as

$$E_{\text{CNT}} = \sum_i \sum_{j(>i)} [V_{\text{R}}(r_{ij}) - \bar{B}_{ij} V_{\text{A}}(r_{ij})] \quad (2)$$

in which  $r_{ij}$  is the distance between atom  $i$  and  $j$ ,  $V_{\text{R}}(r_{ij})$  and  $V_{\text{A}}(r_{ij})$  are Morse type pair potential terms that account for repulsive and attractive interactions between atom  $i$  and  $j$ , as given below:

$$V_R(r_{ij}) = \frac{f_{ij}(r_{ij})D_{ij}^{(e)}}{(S_{ij} - 1)} e^{-\sqrt{2S_{ij}}\beta_{ij}(r-R_{ij}^{(e)})}, \quad (3)$$

$$V_A(r_{ij}) = \frac{f_{ij}(r_{ij})D_{ij}^{(e)}S_{ij}}{(S_{ij} - 1)} e^{-\sqrt{2S_{ij}}\beta_{ij}(r-R_{ij}^{(e)})}, \quad (4)$$

where  $D_{ij}^{(e)}$ ,  $S_{ij}$ ,  $\beta_{ij}$  and  $R_{ij}^{(e)}$  are model constants, formulated for each atom in the covalent bond. Function  $f_{ij}(r_{ij})$  accounts for bond stretching and breaking and assumes the following form

$$f_{ij}(r) = \begin{cases} 1, & r < R_{ij}^{(1)} \\ \left[ 1 + \cos\left(\frac{\pi(r-R_{ij}^{(1)})}{(R_{ij}^{(2)}-R_{ij}^{(1)})}\right) \right] / 2, & R_{ij}^{(1)} < r < R_{ij}^{(2)} \\ 0, & r > R_{ij}^{(2)} \end{cases} \quad (5)$$

with  $R_{ij}^{(1)}$  and  $R_{ij}^{(2)}$  being the cut-off lengths for bond stretching and breaking, respectively.

$\bar{B}_{ij}$  in Eq. (2) is referred to as the bond order term. It is an average of the terms associated with each atom participating in the bond and a correction term, primarily dependent on the number of bonds linked to atoms  $i$  and  $j$ . In the case for  $sp^2$  hybridized carbon, the correction term is zero and therefore  $\bar{B}_{ij}$  is given as

$$\bar{B}_{ij} = \frac{(B_{ij} + B_{ji})}{2}. \quad (6)$$

The bonding angle effect is reflected in the term  $B_{ij}$ , which is

$$B_{ij} = \left[ 1 + \sum_{k(\neq i,j)} G_i(\theta_{ijk}) f_{ik}(r_{ik}) e^{\alpha_{ijk}[(r_{ij}-R_{ij}^{(e)})-(r_{ik}-R_{ik}^{(e)})]} \right]^{-\delta_i}. \quad (7)$$

The term  $\theta_{ijk}$  is the angle between two adjacent covalent bonds that links atom  $i$  to  $j$  and  $i$  to  $k$ . The parameter  $\alpha_{ijk}$  is zero for pure C–C systems. The function  $G_i(\theta)$ , for carbon, is given below with  $c_0$  and  $d_0$  as constants:

$$G_C(\theta) = a_0 \{ 1 + c_0^2/d_0^2 - c_0^2/[d_0^2 + (1 + \cos \theta)^2] \}. \quad (8)$$

Two sets of constants have been used for the Brenner potential, both can be found in [25]. The parameter set 1 from [25] is used for all the CNTs in the simulations performed. It has been shown that parameter set 1 gives better fit for the equilibrium bond length than parameter set 2.

## 2.2. Force field for polymers

The polymer systems are modeled using DL\_POLY [26] force field. The DL\_POLY force field representation of PE incorporates four interatomic potentials: bond, valence angle, dihedral angle and 1–4 interaction. The only intermolecular potential accounted is the short ranged (van der Waals) potential. Electrostatic (Coulombic) forces are not taken into account. The total energy of the polyethylene matrix can be expressed as:

$$E_{\text{polyethylene}} = E_{\text{bond}} + E_{\text{angle}} + E_{\text{dihedral}} + E_{\text{short-ranged}}. \quad (9)$$

The terms in the above expression are explained in the following equations from the DL\_POLY force field. Fig. 1 illustrates the definition of the three bonded interactions.

(a) The bond potential is given as a Morse potential:

$$U(r_{ij}) = E_0 \left[ \{ 1 - e^{-k(r_{ij}-r_0)} \}^2 - 1 \right], \quad (10)$$

where  $r_{ij}$  is the bond length,  $E_0$  and  $k$  are constants, and  $r_0$  is the equilibrium bond length. The parameters used for various bonds are listed in Table 1.

(b) Valence angle potential is expressed in the form of harmonic cosine:

$$U(\theta_{jik}) = \frac{\bar{k}}{2} (\cos(\theta_{jik}) - \cos(\theta_0))^2, \quad (11)$$

where  $\theta_{jik}$  is the angle between the two bonds,  $\bar{k}$  a constant and  $\theta_0$  the equilibrium value of the angle. The parameters used for the various valence angles in the system are given in Table 2.

(c) Dihedral angle (Cosine potential):

$$U(\phi_{ijkn}) = A[1 + \cos(m \cdot \phi_{ijkn} - \delta)], \quad (12)$$

where  $\phi_{ijkn}$  is the dihedral angle,  $A$ ,  $m$  and  $\delta$  are constants. The parameter values used for all the dihedral interactions in the PE system are given in Table 3. Note the difference

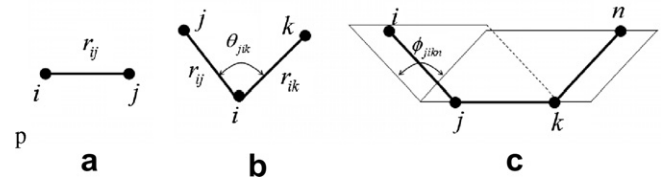


Fig. 1. Definition of: (a) bond potential, (b) valence angle potential and (c) dihedral potential.

Table 1  
Parameters for bond (Morse) potential

Parameter	C–C bond	C–H bond	Units
$E_0$	70.000	70.000	kcal/mol
$r_0$	1.53	1.09	Å
$k$	2.236	2.236	(Å) <sup>-1</sup>

Table 2  
Parameters for valence angle (Harmonic Cosine) potential

Parameter	C–C–C	H–C–H	C–C–H/H–C–C	Units
$\bar{k}$	112.5	112.5	112.5	kcal/mol
$\theta_0$	109.47	109.47	109.47	rad

Table 3  
Parameters for dihedral angle (Cosine) potential

Parameter	H–C–C–H/H–C–C–C (terminal C atom)	C–C–C–H/C–C–C–C (internal C atom)	Units
$A$	0.1667	0.1111	kcal/mol
$\delta$	0	0	rad
$m$	3	3	–

Table 4  
Parameters for L–J potential

Interaction type	Parameter	
	$A$ (kcal/mol $\text{\AA}^{12}$ )	$B$ (kcal/mol $\text{\AA}^6$ )
C–C	802442.06	460.584
C–H	150602.42	151.339
H–H	17198.63	32.337

between a terminal and internal carbon. A terminal carbon atom in a PE chain is bonded to one C and three H atoms, while an internal carbon atom is bonded to two C and two H atoms, hence the difference in the dihedral values. In addition, two more parameters are used to control the non-bonded forces acting between the 1st and the 4th atoms defining the dihedral. These interactions are called 1–4 interactions and use the same potentials defined for the rest of the short-ranged interactions. These potentials are described in the following subsection.

### 2.3. Interaction model between carbon nanotubes and polymer

The DL\_POLY [26] force field incorporates potentials for non-bonded as well as intermolecular interactions. In our system, the only interactions between the two materials are the non-bonded or van der Waals (vdW) forces. Lennard–Jones [27] (L–J) potential is the potential of choice for all vdW interactions in our system. L–J parameters reported by Girifalco [28] for carbon–carbon systems are used for all vdW interactions involving carbon atoms. The L–J potential equation is given below:

$$U(r_{ij}) = 4\epsilon \left[ \left( \frac{\sigma}{r_{ij}} \right)^{12} - \left( \frac{\sigma}{r_{ij}} \right)^6 \right], \quad (13)$$

where  $r_{ij}$  is the distance between the non-bonded pair of atoms,  $\epsilon$  and  $\sigma$  are constants. The L–J potential can be simplified and implemented as the so-called 12–6 potential, which is

$$U(r_{ij}) = \left[ \frac{A}{(r_{ij})^{12}} - \frac{B}{(r_{ij})^6} \right]. \quad (14)$$

The parameters  $A$  and  $B$  used for different atom-pair combinations are reported in Table 4.

### 3. Molecular structures

All the CNT-based composite systems studied in this paper can be categorized as single-walled CNTs embedded in either crystalline or amorphous PE matrix. The open-ended or capped nanotubes used in all the composite systems are (10, 10) armchair nanotubes, unless otherwise specified. The atomic structure and connectivity of PE is generated based on the logic in DL\_POLY Java GUI [26] code. Detailed procedures follows these described in [26].

In the case of generating crystalline PE structure, an orthorhombic unit cell of crystalline PE is initially generated using the parameters reported in [29]. The cell parameters corresponding to the DL\_POLY force field were calculated. The generated structure is further relaxed to an equilibrium configuration and the parameters at this configuration are noted. The orthorhombic unit cell is then replicated periodically in all three directions to obtain the structure corresponding to the actual simulation cell. The generated rectangular parallelepiped simulation cell is periodic in all the three directions automatically. For the purpose of simplicity, the chains are always generated parallel to the Z-axis (same as the tube axis, shown in Fig. 2).

The density obtained for the equilibrium structure of linear PE chains, considering each chain as a single molecule, is  $0.9 \text{ g/cm}^3$ . The density of the equilibrium configuration of amorphous PE is calculated assuming that all the atoms in the simulation cell constitute a single molecule of polyethylene. A density of  $0.9 \text{ g/cm}^3$  is obtained for random PE chains, which is exactly the same as that for linear PE chains. This indicates the consistency in the two structures and verifies the molecular representation used for modeling them. These values also match perfectly with the values reported for LDPE and LLDPE in [30].

In the case of composites, the CNT is generated separately from the crystalline PE structure. The coordinates for the two structures are merged, ensuring that the CNT is centered within the polymer structure. The radius of the CNT is calculated and PE chains within this radius are removed, replacing them with the CNT. An initial gap of 3–4  $\text{\AA}$  is introduced between the CNT and the clos-

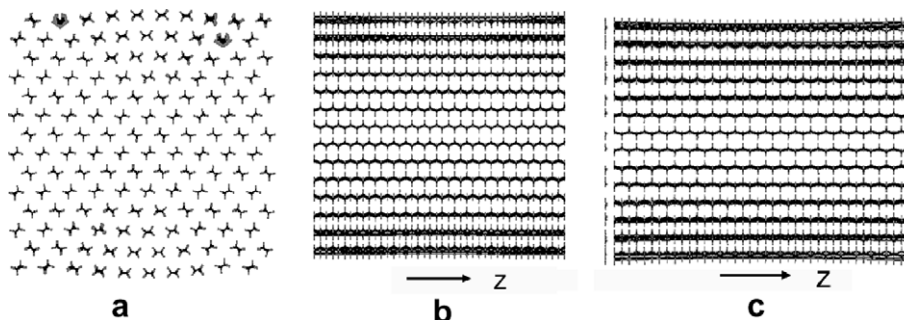


Fig. 2. Longitudinal tensile loading of crystalline polyethylene (aligned chains): (a, b) equilibrium structure and (c) structure at fracture.

est PE chains by removing the PE chains. After the initial configurations are introduced, the gap between the CNT and PE will be further adjusted by relaxing the system using MM. This ensures the equilibrium of the system before any force is applied.

The amorphous PE structure is generated by a random walk algorithm. The chain is started with a single ethylene unit. One hydrogen atom from this unit is replaced by the carbon atom from another, hence propagating the chain. Each monomer unit added is ensured to be energetically stable and not overlapping any of the previously added units. This algorithm was modified to seed the chain randomly inside the specified volume and also to incorporate a completely enclosed cavity without having to break the chain. For a through cavity, no monomer units would be generated in a cylindrical region of the specified radius. In the case of an enclosed cavity, the length of the cylindrical region to exclude, shorter than the simulation cell, would be additionally specified. The algorithm ensures that the cavity is placed at the center of the rectangular parallelepiped unit cell. In some structures, noticeable voids or pockets were observed even though the addition of new monomer units had ceased, typically caused by the propagating end of the random chain getting trapped inside previously added units. The simulation cell generated is periodic in all the directions and the single chain generated is infinitely long because of the periodic condition. Further modifications to the connectivity are made such that all the simulation cells used for tensile or pull-out simulations are non-periodic.

#### 4. Simulation concepts and setup

Energy minimization based on the L-BFGS-B [31] algorithm is used throughout this study. The tensile simulations presented are modeled by a quasi-static, displacement update scheme. Tensile boundary conditions similar to mechanical testing are modeled to determine the tensile strength and elastic moduli of polymer and composite systems. Similar to pull-out, one end of the simulation cell is constrained while an incremental displacement is applied to the atoms at the other end. In the case of crystalline PE, only one layer of atoms from each chain will constitute the boundary, while in the case of amorphous PE, a slab of atoms constitutes the boundary. For composite systems with a through CNT, a single ring of atoms marks the boundary of the CNT, while the CNT does not contribute to the boundary layer if it is completely embedded.

The tensile strengths are calculated from the total force acting on the boundary atoms, in the direction of applied displacement, per unit area of the cross-section. The Young's moduli reported throughout the study are calculated as the average of the slope of the stress–strain curve in the linear region (<4% strain). In the case of transverse loading of crystalline PE structure, the region of linear response is smaller and therefore a smaller region is used.

For crystalline PE-through CNT models, one end of the CNT and all polymer chains were fixed and an incremental displacement was applied to the other end. For amorphous PE-through CNT models, one end of the CNT and a 5 Å slab of polymer atoms were fixed on one side and an incremental displacement was applied on the other end of the CNT and a 5 Å polymer slab. For CNT embedded in amorphous PE matrix, the CNT is completely inside the matrix and does not form a part of the boundary. In this case, 5 Å slabs of polymer atoms on either ends are constrained as the boundary of the simulation cell. The width of 5 Å is chosen to be the minimal slab width such that applied boundary condition can be transmitted into the entire PE structure.

### 5. Simulations, results and discussions

#### 5.1. Uniaxial tensile loading of pure crystalline polyethylene

Aligned chains of polyethylene were relaxed to an energetically stable state and then subjected to tensile boundary conditions. One end of each chain was fixed and the other end was subjected to incremental longitudinal displacement (0.1 Å per step for 265 steps), relaxing the structure to equilibrium in each loading step. The simulation cell is 46 Å × 47 Å × 53 Å, with 17,640 atoms and the polymer chains are parallel to the Z-direction. The equilibrium and fractured structures are shown in Fig. 2. Fracture occurs simultaneously at the two ends.

As is evident from the corresponding stress–strain plot in Fig. 3, the polymer chains fracture at ~22% engineering strain, without exhibiting much plastic deformation. At the point of fracture, all the chains break simultaneously. The nature of the simulation is strongly governed by the inter-atomic potentials. In this case, the force field indicates a lack of plasticity along the chain direction for polyethylene.

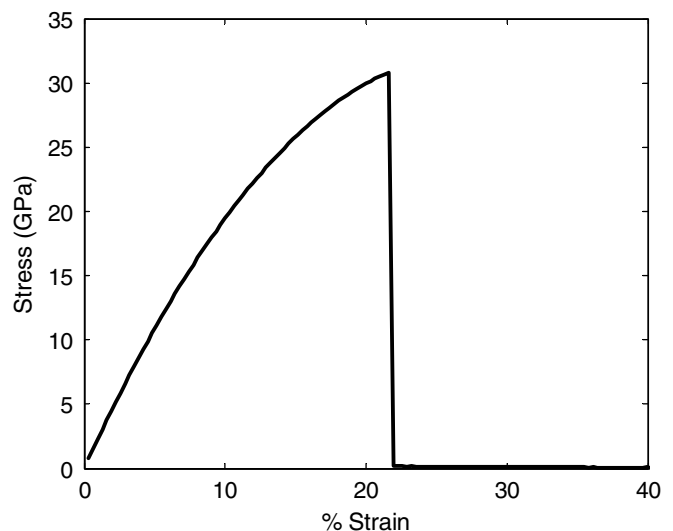


Fig. 3. Engineering stress versus strain for longitudinal tensile loading of crystalline polyethylene.

Young's moduli ( $C_{33}$ ) of 212–215 GPa are obtained, which fits well with the *experiment* (150–180 GPa [30]). Previously studies using *ab initio method* (320 GPa [32], 334 GPa [33]) and *density functional theory* (347–405 GPa [34]) seem to have overestimated this value. A tensile strength of 30.82 GPa is obtained along the chains.

A smaller unit cell of the crystalline PE structure is subjected to transverse tensile loading. The simulation cell is  $37 \text{ \AA} \times 34 \text{ \AA} \times 30 \text{ \AA}$ , with 6000 atoms. The equilibrium structure of the cell and the structure after 40% strain in  $X$  and  $Y$  directions are shown in Fig. 4. The plots in Fig. 5 depict the nature of the stress generated in the polymer structure versus the applied engineering strain. The strain applied on the boundary atoms is observed to cause extensive interlayer sliding and twinning as the polymer deforms. The Young's moduli obtained in the  $X$  and  $Y$  directions ( $C_{11}$  and  $C_{22}$ ) are 10 and 12 GPa, respectively. The corresponding tensile strengths are 0.38 and 0.26 GPa, respectively. These values match closely with those reported in [29] – 14.1 GPa ( $C_{11}$ ) and 11.8 GPa ( $C_{22}$ ). The discrepancies are due to the fact that *ab initio method* was implemented on a unit cell of five PE chains in [29]. In contrast, a cell of 80 chains is considered in the current system. As shown in Fig. 4a, the relaxed crystalline PE structure does not show a clear pattern of period-

icity. Thus the periodical condition used in [29] is not directly applicable to the system here. The fact that no bonded interactions resist the strain and deformation in transverse direction explains the high degree of anisotropy in crystalline PE.

## 5.2. Uniaxial tensile loading of pure amorphous polyethylene

In the next set of simulations, random polyethylene chains are subjected to tensile loading. Since the system under investigation is not periodic, the non-bonded atoms on the boundaries are eliminated. The simulation cell size for this structure is  $45 \text{ \AA} \times 45 \text{ \AA} \times 44 \text{ \AA}$  and has 11,240 atoms. The initial structure is relaxed in multiple stages and a 5 Å slab of boundary atoms is constrained to apply tensile boundary conditions. The amorphous PE structures at equilibrium and at ~120% strain are shown in Fig. 6. The nature of engineering stress versus engineering strain for the amorphous PE structure is depicted in Fig. 7a and matches closely with the shape of the curve reported in [30]. The elastic moduli ( $C_{11}$ ,  $C_{22}$  and  $C_{33}$ ) and tensile strengths for this structure are reported in Table 5. The fact that the Young's modulus is similar in all the three directions firmly supports the isotropic nature of amorphous PE.

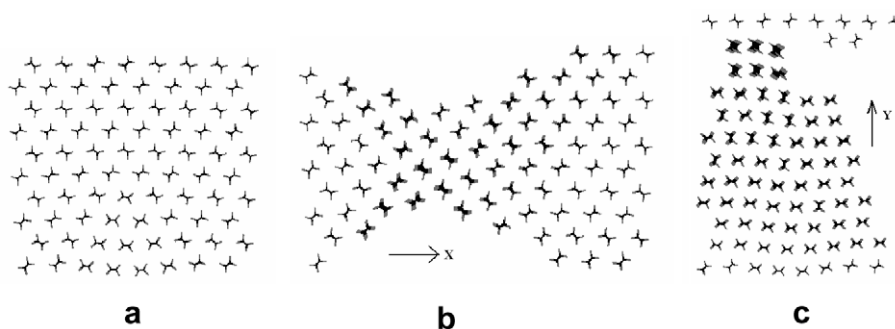


Fig. 4. Transverse tensile loading of crystalline polyethylene (aligned chains): (a) equilibrium structure, (b) 40% strain along  $X$  and (c) 40% strain along  $Y$  directions.

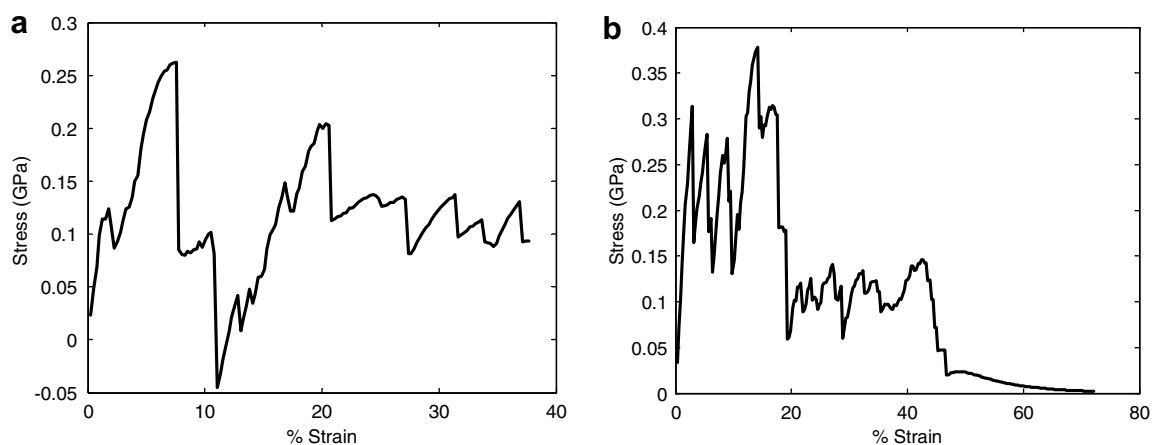


Fig. 5. Engineering stress versus strain for transverse tensile loading of crystalline polyethylene: (a)  $X$  direction and (b)  $Y$  direction.

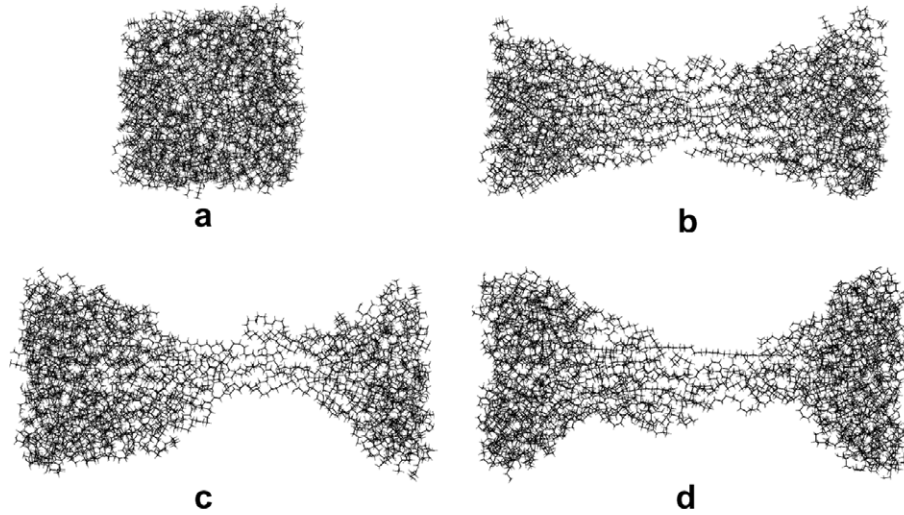


Fig. 6. Tensile loading of amorphous polyethylene (random chains): (a) equilibrium structure, (b) 120% strain in X direction, (c) 120% strain in Y direction and (d) 120% strain in Z direction.

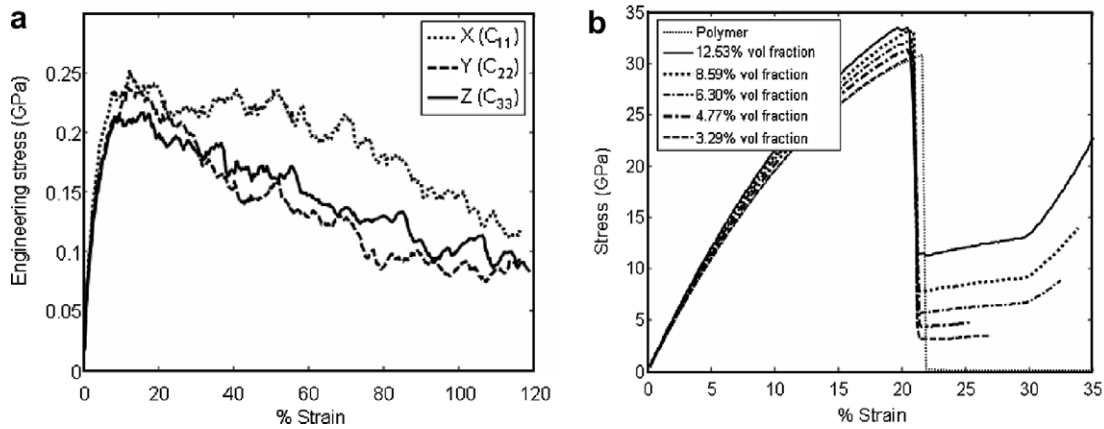


Fig. 7. Engineering stress versus strain plots for tensile loading of: (a) amorphous polyethylene, (b) composite with through nanotube in crystalline polyethylene matrix.

Table 5  
Elastic moduli and tensile strength of amorphous polyethylene (random chains)

Direction	Elastic modulus (GPa)	Tensile strength (GPa)
X	( $C_{11}$ ) 3.6975	0.2526
Y	( $C_{22}$ ) 3.1902	0.2375
Z	( $C_{33}$ ) 3.2164	0.2170

5.3. Uniaxial tensile loading of crystalline PE reinforced by through CNT

Composite structures with through CNTs in linear PE chains are studied using similar boundary conditions as that for pure PE. Different volume fraction ratios are tried and the comparison of results is presented in Fig. 7b. The Young’s modulus and tensile strength for each volume fraction ratio and increase over pure PE are given in Table 6. Based on MM simulation of uniaxial tensile test of the (10, 10) CNT, the Young’s modulus and Poisson’s ratio

of the (10, 10) CNT are calculated to be 0.86 TPa and 0.19, respectively. The volume fraction calculations assume that the CNT can be considered as a solid cylinder, not a hollow tube.

As can be observed from Table 6, the increase in Young’s modulus of the composite over pure PE is much

Table 6  
Young’s moduli and tensile strengths of crystalline PE reinforced by long through CNT

CNT volume fraction (%) solid/hollow	Young’s modulus (GPa)	Tensile strength (GPa)	% Increase in Young’s modulus	Rule of mixture calculations (GPa) solid/hollow
0/0	214.76	30.82	0	214.76/214.76
3.29/2.11	217.51	30.56	1.28	235.82/228.27
4.77/3.06	223.16	31.29	3.91	245.30/234.33
6.3/4.04	228.52	32.35	6.41	255.10/240.63
8.58/5.50	233.52	33.21	8.74	269.69/249.98
12.53/8.03	237.78	33.48	10.72	294.98/266.18

Volume fraction is evaluated based on solid/hollow cylinder assumption.

less than expected, even though the volume fraction of nanotubes is relatively high. This is evident from the fact that the modulus of CNTs is just four times that of linear PE chains. These values are not in agreement with the calculations by the rule of mixtures, since the deviation introduced by the continuum definition of CNT is high. For the rule of mixture calculations, the effective volume of the CNT is calculated by adding half the average distance between the CNT and the polymer to the CNT radius. The volume of the polymer is calculated by subtracting the effective CNT volume from the total volume of the simulation cell. If the CNT is represented as a hollow cylinder and the inner volume of this cylinder is deducted from the total volume of the composite cell, the results vary significantly (Table 6). These results match more closely with rule of mixtures than those with solid cylinder assumption for the nanotube. The fractured structures for different volume fractions of the CNT are shown in Fig. 8. Chain breaking is observed to be completely random, with some chains breaking near the boundary while some fracture near the center. The increase in the stress after fracture corresponds to the fact that the CNT is still intact and hence bears the load.

#### 5.4. Uniaxial tensile loading of amorphous PE reinforced by through CNT

A composite system with amorphous PE and a through CNT is subjected to tensile loading to calculate the

increase in Young's modulus over pure PE. Tensile boundary conditions are applied on a 5 Å slab of the cell. As can be observed from Fig. 9, due to the high plasticity and low elastic modulus of amorphous PE, maximum stress is generated in the CNT and it fractures before the polymer. The engineering stress versus applied strain for this system is plotted in Fig. 10. The nature of this plot matches closely with that for Brenner potential [35] and justifies that most of the stress is borne by the CNT. The effective Young's modulus is 82 GPa for 11.25% volume fraction (with solid cylinder assumption, 7.22% volume fraction by hollow cylinder assumption), which is roughly 25 times of that obtained for pure amorphous PE. The tensile strength for this system is 46 GPa, more than 100 times increase over pure PE. We observe that the failure strain in this case is about 35%. This is close to the 30% failure strain as obtained in [36] on CNT without any defects.

Two important aspects regarding composites with through CNTs are worth mentioning here. Firstly, it is still a challenge to realize such composite systems. Carbon nanotubes, long enough for structural applications, are difficult to synthesize and bulk production of such CNTs is still being pursued. Secondly, for amorphous as well as crystalline polymer, there is negligible load transfer at the nanotube–polymer interface. Both the materials bear the axial load independently of each other. This was confirmed by the fact that disabling vdW interactions between CNT atoms and polymer atoms did not

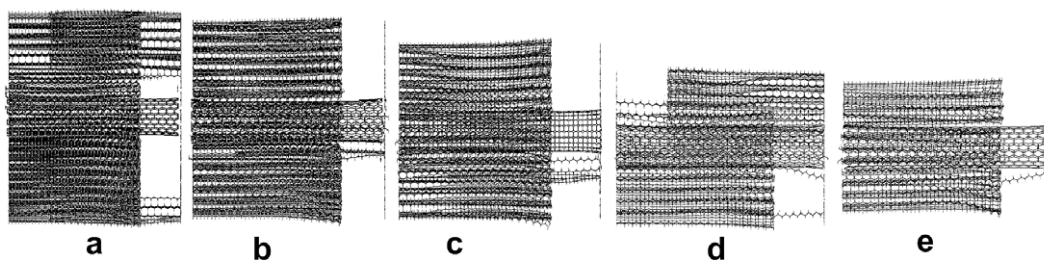


Fig. 8. Fracture in tensile loading of CNT–crystalline PE composite for volume fractions of (solid cylinder assumption): (a) 3.29%, (b) 4.77%, (c) 6.3%, (d) 8.58% and (e) 12.53%.

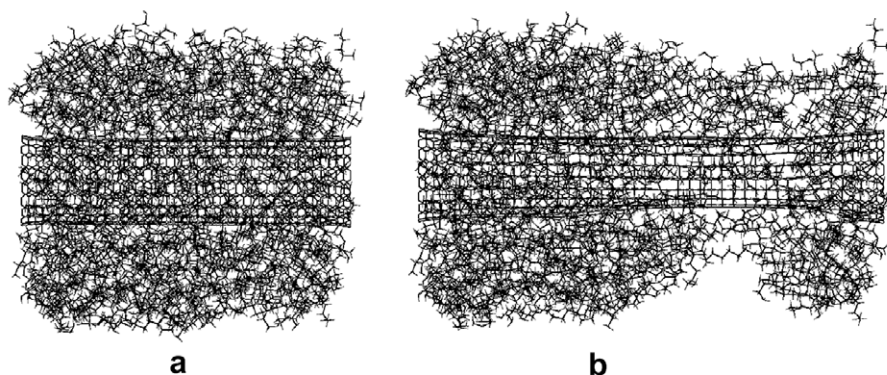


Fig. 9. Tensile loading of nanotube–polyethylene (amorphous) composite: (a) equilibrium structure, (b) structure at nanotube fracture (~35% strain).

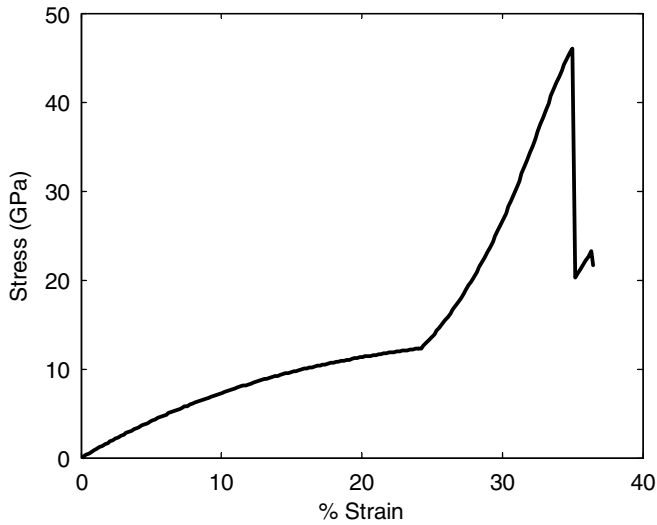


Fig. 10. Engineering stress versus strain for longitudinal tensile loading of composite with through nanotube in amorphous polyethylene matrix (volume fraction 11.25%).

result in any noticeable change in the effective Young’s modulus of the composite system using the current models.

Table 7  
Young’s moduli and tensile strengths of amorphous PE reinforced by short CNT

% Volume fraction	Young’s modulus (GPa)	Tensile strength (GPa)
0	3.2164	0.2170
1.4608	1.6588	0.0734
1.8627	1.8686	0.0972
3.0522	2.3230	0.0902
3.5948	2.2217	0.1246
6.3386	2.5447	0.1620
6.9206	2.8802	0.1624

5.5. Uniaxial tensile loading of amorphous PE reinforced by short CNT

For the next set of simulations, composite systems with capped single-walled nanotubes are simulated to calculate the increase in tensile strength and Young’s modulus over pure PE. The 62 Å long (10, 10) nanotube is completely embedded inside the random PE matrix and capped using hemispherical sections of C<sub>240</sub> molecule. The PE chains are propagated surrounding the enclosed cavity for the nanotube, ensuring that no less than 15 Å layer of PE is generated surrounding it. As for the previous systems, the non-bonded atoms on the boundary are eliminated and tensile boundary conditions are applied over a 5 Å slab on either side of the composite cell. The change in Young’s

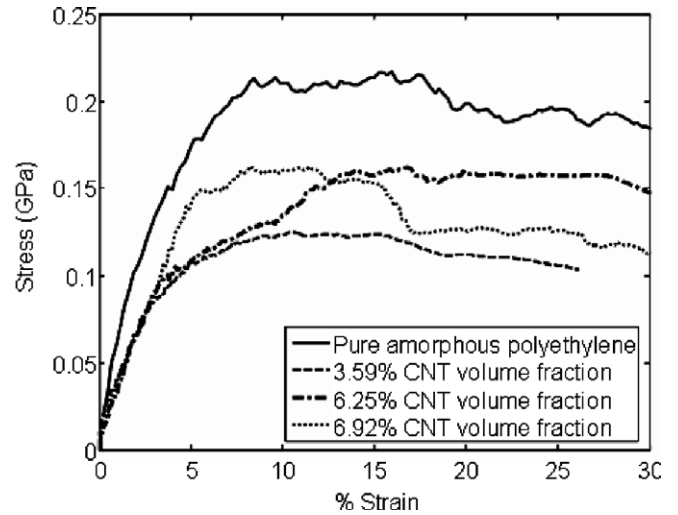


Fig. 12. Engineering stress versus strain plots for amorphous polyethylene and embedded nanotube composite systems.

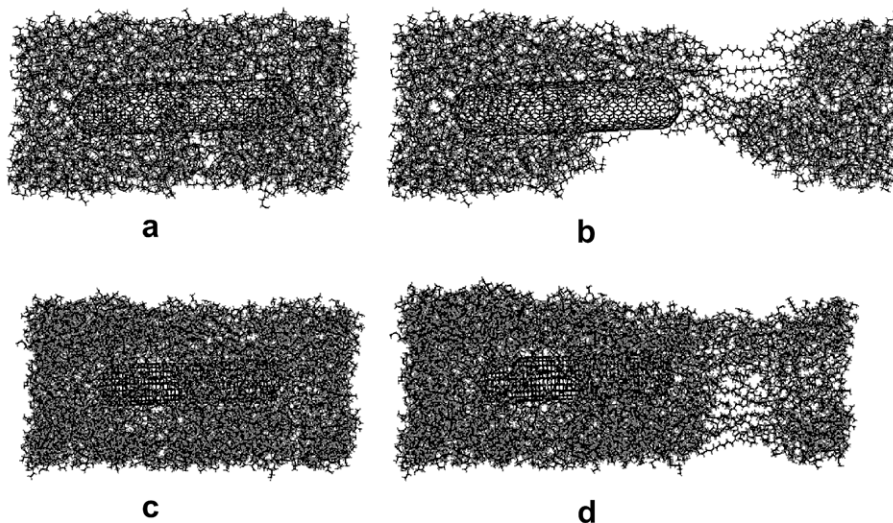


Fig. 11. Tensile loading of embedded nanotube–amorphous PE composite: (a) equilibrium structure (6.25% volume fraction), (b) corresponding structure (a) at 45% strain, (c) equilibrium structure (3.59% volume fraction), (d) corresponding structure (c) at 26% strain.

modulus and tensile strength values over pure PE, for different volume fractions of CNT, are given in Table 7.

The equilibrium structures of two composite systems, 6.25% and 3.59% CNT vol. fraction, are shown in Fig. 11a and c, respectively. The structure in (a) at 45% strain is shown in (b) and the structure in (c) at 26% strain is shown in (d). Comparison graphs for engineering stress versus strain for different volume fractions with short, embedded CNT are depicted in Fig. 12. The tensile strength of the composite is less than pure amorphous PE, since the contact area of the CNT–PE interface is too small for effective load transfer. Although an estimate on the critical length for effective load transfer to CNT in amorphous PE matrix is not available at the time, we expect this to be on the order of microns, as in the case of nanoropes [37]. The short, embedded CNT may act like a void, reducing the tensile strength of the matrix. The CNT volume fraction does not indicate a significant influence on the composite strength.

## 6. Conclusions

The elastic moduli and tensile strengths of crystalline and amorphous PE are determined based on MM simulation, which compare well with results reported in the literature. The highly anisotropic nature of linear PE chains and isotropic nature of amorphous PE is clearly seen from our results. Based on MM simulation results, it is observed that the tensile strength of well-aligned crystalline PE, along the linear chains, is very high and of same order as the nanotubes. This, however, does not necessarily imply that crystalline PE can be readily used in applications. As shown in [38], the synthesized crystalline PE has been in the form of polycrystal and a mixture with amorphous PE always presents.

The increase in strength by reinforcing the crystalline PE, even with a through CNT, is not significantly high. On the other hand, reinforcing an amorphous PE matrix with a through CNT increases its elastic modulus and tensile strength by a large factor. This increase is justified by the fact that the CNT is much stiffer and bears most of the load. The properties at the CNT–PE interface play no role in governing the properties of composites with through CNTs. The two materials bear the load independent of each other. This was verified by the fact that properties of a composite with through CNT in crystalline PE does not change by turning off the non-bonded forces acting at the interface. Although a work in progress, polymer composites with through CNTs are difficult to realize at this stage since the lengths of commercially available CNTs are only of the order of millimeters.

Amorphous PE composite with short CNTs is close to the nanocomposite structure currently being synthesized. With the addition of short CNTs to the PE matrix, the Young's modulus and tensile strength of the composite are significantly less than that of pure PE. This indicates poor load transfer from the matrix to CNT. Although an

exact evaluation on the critical contact length for effective load transfer is not yet available, we estimate it to be on the order of microns based on the previous study on CNT bundles [37]. In addition, we observe that the strength and elastic modulus increases with the increasing volume fraction of CNTs, but the values are lower as compared to pure PE. This phenomenon could be explained if the embedded CNTs were longer than the critical length required for effective load transfer at the interface. The choice of the CNT length in this paper is limited by the computational cost when a pure atomistic approach is used. If coupled with a continuum method, the present computational work can be extended to model contact lengths that are comparable with the experiment. We have recently successfully implemented [39] a combination of this nanoscale approach with microscale continuum models for evaluations of the effective moduli of CNT composites based on a cohesive interface model.

## References

- [1] Iijima S. Helical microtubules of graphitic carbon. *Nature* 1991;354:56–8.
- [2] Thostenson ET, Ren ZF, Chou T-W. Advances in the science and technology of carbon nanotubes and their composites: a review. *Compos Sci Technol* 2001;61:1899–912.
- [3] Qian D, Wagner GJ, Liu WK, Yu MF, Ruoff RS. Mechanics of carbon nanotubes. *Appl Mech Rev* 2002;55(6):495–533.
- [4] Baughman RH, Zakhidov AA, de Heer WA. Carbon nanotubes – the route toward applications. *Science* 2002;297(5582):787–92.
- [5] Qian D, Dickey EC, Andrews R, Rantell T. Load transfer and deformation mechanisms in carbon nanotube–polystyrene composites. *Appl Phys Lett* 2000;76(20):2868–70.
- [6] Wagner HD, Lourie O, Feldman Y, Tenne R. Stress-induced fragmentation of multiwall carbon nanotubes in a polymer matrix. *Appl Phys Lett* 1998;72(2):188–90.
- [7] Schadler LS, Giannaris SC, Ajayan PM. Load transfer in carbon nanotube epoxy composites. *Appl Phys Lett* 1998;73(26):3842–4.
- [8] Bower C, Rosen R, Jin L, Han J, Zhou O. Deformation of carbon nanotubes in nanotube–polymer composites. *Appl Phys Lett* 1999;74(22):3317–9.
- [9] Liu YJ, Chen XL. Evaluations of the effective material properties of carbon nanotube-based composites using a nanoscale representative volume element. *Mech Mater* 2003;35(1–2):69–81.
- [10] Chen XL, Liu YJ. Square representative volume elements for evaluating the effective material properties of carbon nanotube-based composites. *Comp Mater Sci* 2004;29(1):1–11.
- [11] Liu YJ, Nishimura N, Otani Y. Large-scale modeling of carbon-nanotube composites by the boundary element method based on a rigid-inclusion model. *Comp Mater Sci* 2004;34(2):173–87.
- [12] Schadler LS, Giannaris SC, Ajayan PM. Load transfer in carbon nanotube epoxy composites. *Appl Phys Lett* 1998;73(26):3842–4.
- [13] Ajayan PM, Schadler LS, Giannaris C, Rubio A. Single-walled carbon nanotube–polymer composites: strength and weakness. *Adv Mater* 2000;12(10):750–1.
- [14] Ding W, Eitan A, Fisher FT, Chen X, Dikin DA, Andrews R, et al. Direct observation of polymer sheathing in carbon nanotube–polycarbonate composites. *Nano Letters* 2003;3(11):1593–7.
- [15] Xiao KQ, Zhang LC. The stress transfer efficiency of a single-walled carbon nanotube in epoxy matrix. *J Mater Sci* 2004;39(14):4481–6.
- [16] Frankland SJV, Caglar A, Brenner DW, Griebel M. Reinforcement mechanisms in polymer nanotube composites: simulated non-bonded and cross-linked systems. In: *MRS 2000 fall meeting proceedings*; 2000.

- [17] Frankland SJV, Caglar A, Brenner DW, Griebel M. Molecular simulation of the influence of chemical cross-links on the shear strength of carbon nanotube–polymer interfaces. *J Phys Chem B* 2002;106(12):3046–8.
- [18] Frankland SJV, Harik VM. Analysis of carbon nanotube pull-out from a polymer matrix. *Surf Sci* 2003;525(1–3):L103–8.
- [19] Griebel M, Hamaekers J. Molecular dynamics simulations of the elastic moduli of polymer–carbon nanotube composites. *Comput Meth Appl Mech Eng* 2004;193(17–20):1773–88.
- [20] Pipes BR, Hubert P. Helical carbon nanotube arrays: mechanical properties. *Compos Sci Technol* 2002;62(3):419–28.
- [21] Odegard GM, Gates TS, Wise KE, Park C, Siochi EJ. Constitutive modeling of nanotube-reinforced polymer composites. *Compos Sci Technol* 2003;63(11):1671–87.
- [22] Fisher FT, Bradshaw RD, Brinson LC. Effects of nanotube waviness on the modulus of nanotube-reinforced polymers. *Appl Phys Lett* 2002;80(24):4647–9.
- [23] Fisher FT, Bradshaw RD, Brinson LC. Fiber waviness in nanotube-reinforced polymer composites-1: modulus predictions using effective nanotube properties. *Compos Sci Technol* 2003;63(11):1689–703.
- [24] Li CY, Chou TW. Multiscale modeling of carbon nanotube reinforced polymer composites. *J Nanosci Nanotechnol* 2003;3(5):423–30.
- [25] Brenner DW. Empirical potential for hydrocarbons for use in simulating the chemical vapor-deposition of diamond films. *Phys Rev B* 1990;42(15):9458–71.
- [26] Smith W, Forester TR. DL\_POLY\_2.0: A general-purpose parallel molecular dynamics simulation package. *J Mol Graphics* 1996;14(3):136–41.
- [27] Lennard-Jones JE. The electronic structure of some diatomic molecules. *T Faraday Soc* 1929;25:668–86.
- [28] Girifalco LA, Lad RA. Energy of cohesion, compressibility and the potential energy functions of the graphite system. *J Chem Phys* 1956;25(4):693–7.
- [29] Serra S, Iarlori S, Tosatti E, Scandolo S, Santoro G. Dynamical and thermal properties of polyethylene by ab initio simulation. *Chem Phys Lett* 2000;331:339–45.
- [30] Peacock AJ. Handbook of polyethylene: structures, properties, and applications. New York: Marcel Dekker, Inc.; 2000. p. 544.
- [31] Byrd RH, Lu P, Nocedal J. A limited memory algorithm for bound constrained optimization. *SIAM J Sci Stat Comp* 1995;16(5):1190–208.
- [32] Peeters A, Van Alsenoy C, Zhang M-L, Van Doren VE. On the use of supermolecule model for calculation of Young's modulus of crystalline polymers. *Int J Quantum Chem* 2000;80(3):425–31.
- [33] Hageman JCL, Meier RJ, Heinemann M, de Groot RA. Young Modulus of crystalline polyethylene from ab initio molecular dynamics. *Macromolecules* 1997;30(19):5953–7.
- [34] Miao MS, Zhang M-L, Van Doren VE, Van Alsenoy C, Martins José Luís X. Density functional calculations on the structure of crystalline polyethylene under high pressures. *J Chem Phys* 2001;115(24):11317–24.
- [35] Che J, Cagin T, Goddard III WA. Studies of fullerenes and carbon nanotubes by an extended bond order potential. *Nanotechnology* 1999;10(3):263–8.
- [36] Yakobson BI, Campbell MP, Brabec CJ, Bernholc J. High strain rate fracture and C-chain unraveling in carbon nanotubes. *Comp Mater* 1997;8(4):341–8.
- [37] Qian D, Liu WK, Ruoff RS. Load transfer mechanism in carbon nanotube ropes. *Compos Sci Technol* 2003;63(11):1561–9.
- [38] Chelazzi D, Ceppatelli M, Santoro M, Bini R, Schettino V. High-pressure synthesis of crystalline polyethylene using optical catalysis. *Nat Mater* 2004;3(7):470–5.
- [39] Liu YJ, Nishimura N, Qian D, Adachi N, Otani Y, Mokashi V. A boundary element method for the analysis of CNT/polymer composites with a cohesive interface model based on molecular dynamics. *Eng Anal Bound Elem* [in press].